The Astrophysical Journal Supplement Series, 277:9 (9pp), 2025 March https://doi.org/10.3847/1538-4365/adacdf

Energetic Transients Joint Analysis System for Multi-INstrument (ETJASMIN) for GECAM. II. Search, Verification, and Classification of Bursts

Ce Cai[1], Yan-Qiu Zhang[2,3], Shao-Lin Xiong[2], Jin-Peng Zhang[2,3], Ping Wang[2], Shi-Jie Zheng[2], Shuo Xiao[4,5], Qi-Bin Yi[2,6], Yi Zhao[7], Hao-Xuan Guo[2,8], Sheng-Lun Xie[2,9], Wang-Chen Xue[2,3], Chao Zheng[2,3], Jia-Cong Liu[2,3], Chen-Wei Wang[2,3], Wen-Jun Tan[2,3], Yue Wang[2,3], Pei-Yi Feng[2,3], Zheng-Hang Yu[2,3], Peng Zhang[2,10], Yan-Ting Zhang[2], Wen-Long Zhang[2,11], Xiao-Yun Zhao[2], Zhen Zhang[2], Xiang Ma[2], Yue Huang[2], Xiao-Bo Li[2], Cheng-Kui Li[2], Ming-Yu Ge[2], Shu-Xu Yi[2], Hai-Sheng Zhao[2], Jin Wang[2], Bing Li[2], Li-Ming Song[2], Lian Tao[2], Shu Zhang[2], and Shuang-Nan Zhang[2,3]

[1] College of Physics and Hebei Key Laboratory of Photophysics Research and Application, Hebei Normal University, Shijiazhuang, Hebei 050024, People's Republic of China; caice@hebtu.edu.cn
[2] Key Laboratory for Particle Astrophysics, Institute of High Energy Physics, Chinese Academy of Sciences, 19B Yuquan Road, Beijing 100049, People's Republic of China; xiongsl@ihep.ac.cn
[3] University of Chinese Academy of Sciences, Chinese Academy of Sciences, Beijing 100049, People's Republic of China
[4] School of Physics and Electronic Science, Guizhou Normal University, Guiyang 550001, People's Republic of China
[5] Guizhou Provincial Key Laboratory of Radio Astronomy and Data Processing, Guizhou Normal University, Guiyang 550001, People's Republic of China
[6] School of Physics and Optoelectronics, Xiangtan University, Xiangtan 411105, People's Republic of China
[7] School of Computer and Information, Dezhou University, Dezhou 253023, Shandong, People's Republic of China
[8] Department of Nuclear Science and Technology, School of Energy and Power Engineering, Xi'an Jiaotong University, Xi'an 710049, People's Republic of China
[9] Institute of Astrophysics, Central China Normal University, Wuhan 430079, People's Republic of China
[10] College of Electronic and Information Engineering, Tongji University, Shanghai 201804, People's Republic of China
[11] School of Physics and Physical Engineering, Qufu Normal University, Qufu, Shandong 273165, People's Republic of China
Received 2024 September 25; revised 2024 December 24; accepted 2025 January 20; published 2025 February 19

Abstract

The Gravitational Wave High-energy Electromagnetic Counterpart All-sky Monitor (GECAM) is a dedicated mission consisting of multiple instruments on different spacecraft to monitor gamma-ray transients. To meet the requirement of GECAM, we developed the Energetic Transients Joint Analysis System for Multi-INstrument (ETJASMIN) pipeline, which has been extended to incorporate other instruments (such as Fermi-GBM, SVOM/GRM). In this work, we introduce the ETJASMIN pipeline with focus on the search, verification, and classification of gamma-ray transients (especially weak bursts) using data from GECAM-B, GECAM-C, and Fermi-GBM. For this pipeline, we implement a coherent algorithm to search for simultaneous signals in the light curves of multiple instruments, conduct a series of Monte Carlo simulations, and validate the pipeline performance with in-flight observation data. The results demonstrate that ETJASMIN can yield not only higher significance of burst search but also more reliable verification and classification of bursts jointly with multiple instruments compared to those derived with an individual instrument. Thus, ETJASMIN is particularly suitable for the exploitation of gamma-ray transients associated with multimessenger multiwavelength sources.

Unified Astronomy Thesaurus concepts: Astronomy data analysis (1858); Gamma-ray detectors (630); Gamma-ray transient sources (1853)

1. Introduction

The Gravitational Wave High-energy Electromagnetic Counterpart All-sky Monitor (GECAM) originally consisted of two microsatellites, GECAM-A and GECAM-B, with a low-Earth-orbit height of 600 km and an inclination angle of 29°, launched in 2020 December 10 (X. Q. Li et al. 2022; C. Wang et al. 2024a). Each satellite carries 25 gamma-ray detectors (GRDs; P. Lv et al. 2018; Z. H. An et al. 2022) and eight charged particle detectors (CPDs; Y. B. Xu et al. 2022). The GRDs operate in the energy range of about 10 keV−5 MeV for measuring the gamma rays (e.g., Y.-P. Chen et al. 2022; Z.-H. An et al. 2023; H.-S. Zhao et al. 2023; Y.-Q. Zhang et al. 2024) and particles (D. L. Zhang et al. 2022), while the CPDs are sensitive to charged particles from about 300 keV to 5 MeV (Y. B. Xu et al. 2022). As a new member of the GECAM mission, GECAM-C (or High Energy Burst Searcher (HEBS)) on board the Space Advanced Technology demonstration satellite (SATech-01), launched on 2022 July 27 (X. Qie et al. 2021), is designed to detect gamma-ray transients in the energy range of about 6 keV−6 MeV (D. Zhang et al. 2023; Y.-Q. Zhang et al. 2023; C. Zheng et al. 2024). The Gamma-ray Transient Monitor (GTM) is an all-sky monitor to detect gamma-ray transients within the energy range of about 10 keV−1 MeV, which was launched on board the Distant Retrograde Orbit-A satellite on 2024 March 13. Since the GTM largely inherits the hardware, software, and scientific operations of the GECAM mission, it is designated as GECAM-D within the GECAM family (P.-Y. Feng et al. 2024; C. Wang et al. 2024b).

The Energetic Transients Joint Analysis System for Multi-INstrument (ETJASMIN[12]) is a dedicated pipeline originally designed for the GECAM series instruments (S. Xiao et al. 2022), to integrate basically all types of data analysis related to gamma-ray transients, including burst search, verification,

[12] We are planning to make the pipeline available in the future once it has been finalized and thoroughly validated.

classification, positional (localization), spectral, and temporal analyses of bursts. The localization, spectral, and temporal analyses of this ETJASMIN pipeline have been extended to other gamma-ray burst (GRB) instruments, including Insight-HXMT/HE (X. Cao et al. 2019; Y. Chen et al. 2019; C. Z. Liu et al. 2019; S. N. Zhang et al. 2019), Fermi-GBM (C. Meegan et al. 2009), Swift-BAT (S. D. Barthelmy et al. 2005), INTEGRAL/SPI-ACS (A. Rau et al. 2005), Konus-Wind (R. L. Aptekar et al. 1995), and GRID (J. Wen et al. 2019), as described in the first paper of this series (S. Xiao et al. 2022, hereafter Paper I). As the second paper of this series for the ETJASMIN pipeline, we focus on the burst search, verification, and classification analyses.

The sensitive search method of gamma-ray transients is critically important in the multimessenger and multiwavelength era for finding weak bursts, especially for those associated with gravitational waves (GWs) or fast radio bursts (FRBs), like GRB 170817A (B. P. Abbott et al. 2017; A. Goldstein et al. 2017; V. Savchenko et al. 2017; T. Li et al. 2018) and the X-ray burst XRB 200428 from the Galactic magnetar SGR J1935+2154 (C. D. Bochenek et al. 2020; CHIME/FRB Collaboration et al. 2020; S. Mereghetti et al. 2020; C. K. Li et al. 2021; A. Ridnaia et al. 2021; M. Tavani et al. 2021).

GECAM has the real-time trigger and localization software operating on board (X.-Y. Zhao et al. 2021). This onboard software looks for signals with an excess signal-to-noise ratio (SNR) in GRDs, which has been utilized by most GRB missions, such as Fermi-GBM (A. von Kienlin et al. 2020) and Insight-HXMT (C. Cai et al. 2021b, 2022b). A coherent method (L. Blackburn et al. 2015) is proposed for the ground-based pipeline to derive a more sensitive search of GBM (A. Goldstein et al. 2016, 2019), GECAM (C. Cai et al. 2025), and other GRB detectors (C. Cai et al. 2021b; M. Kerr et al. 2023) for fainter events that did not trigger on board. The coherent search constructs a likelihood ratio with observed counts and expected counts usually based on the Gaussian statistics, which is a good approximation for the detectors with a sufficient number of counts. We note that, for the cases in which the number of detectors on a single satellite is limited or the burst is rather weak, the number of counts detected would be rather small, which cannot meet the requirements of using Gaussian statistics, and then the Poisson statistics should be used (C. Cai et al. 2023).

In the ETJASMIN pipeline, we try to incorporate all available data of multiple instruments of the GRB missions with similar detector response, including GECAM-A, GECAM-B, GECAM-C, and GBM, to increase the statistics and achieve a higher sensitivity of the burst search. Other instruments, such as GECAM-D and SVOM/GRM (Y. Dong et al. 2010), will be gradually incorporated into this system.

The verification of subthreshold triggers is of great importance but very challenging. For example, a weak event was reported by GBM (V. Connaughton et al. 2016) about 0.4 s after the first GW event (GW150914; B. P. Abbott et al. 2016). The nature of this weak transient has resulted in a vigorous debate because of its low significance (J. Greiner et al. 2016; S. Xiong 2016). In fact, there are a number of subthreshold triggers published with unknown origin from GRB missions, such as Fermi-GBM.[13] With ETJASMIN, we can make a more reliable verification for these weak or even subthreshold triggers using multiple missions.

Furthermore, classification analysis of bursts is essential for GRB missions because they are usually triggered for many reasons, including instrumental effects and bursts from various sources. Doing burst classification with multiple instruments on different spacecraft would make things much easier and reliable. For instance, particle events may occur on a GRB detector when it passes through a region of high particle activity in the orbit, while other instruments operating in regions of low particle flux would remain unaffected. Therefore, combining data from multiple spacecraft offers a promising approach to eliminating the false classification of bursts, like the particle events.

In this paper, we present the methodology, procedures, and preliminary results of the ETJASMIN pipeline, including burst search (Section 2.2), verification (Section 2.3), and classification (Section 2.4). Finally, we give a discussion and conclusion in Section 3.

2. Multi-instrument Joint Analysis

2.1. Data Preparation and Initial Analysis

Since the GRD detectors of GECAM-B and GECAM-C, as well as the NaI detectors of GBM, have similar detector response, the ETJASMIN pipeline integrates data from all these instruments, including event (TTE/EVT) data and the orbital information of the satellites. Additionally, the instrument response for different source locations is also incorporated.

With prior information about the time and/or location of the burst source provided by other instruments, such as LIGO (A. Abramovici et al. 1992) and VIRGO (T. Accadia et al. 2012), we can preliminarily estimate the observation window of each instrument (i.e., whether the source is blocked by Earth or whether the instrument is operational). It is important to note that, in the absence of prior information, only the on-off status of the instrument is considered.

2.2. Burst Search Analysis

2.2.1. Methodology

Following the methodology of the coherent search in L. Blackburn et al. (2015) and C. Cai et al. (2021b), the probability for each detector k to measure the observed data in the presence of a burst signal is defined as

$$P_k(d_k|H_1) = \prod_i \frac{1}{\sqrt{2\pi}\,\sigma_{d_i}} \exp\left(-\frac{(\tilde{d}_i - r_i s)^2}{2\sigma_{d_i}^2}\right), \quad (1)$$

where the product is carried out over each channel i and $\tilde{d}_i = d_i - \langle n_i \rangle$ represents the background-subtracted counts; σ_{d_i} is the standard deviation of the expected data (background + source); r_i represents the instrument response, depending on the direction and energy spectrum of the source; and s is the intrinsic amplitude of the source. The probability for each detector k that the observed counts are simply due to background ($s = 0$) is given by

$$P_k(d_k|H_0) = \prod_i \frac{1}{\sqrt{2\pi}\,\sigma_{n_i}} \exp\left(-\frac{\tilde{d}_i^{\,2}}{2\sigma_{n_i}^2}\right), \quad (2)$$

where σ_{n_i} represents the standard deviation of the background data.

[13] https://gcn.gsfc.nasa.gov/gcn/fermi_gbm_subthresh_archive.html

The log-likelihood ratio (LR) for each detector k and for all detectors is formulated as

$$\mathcal{L}_k = \ln\frac{P_k(d_k|H_1)}{P_k(d_k|H_0)} = \sum_{i=1}\left[\ln\frac{\sigma_{n_i}}{\sigma_{d_i}} + \frac{\tilde{d}_i^{\,2}}{2\sigma_{n_i}^2} - \frac{(\tilde{d}_i - r_i s)^2}{2\sigma_{d_i}^2}\right], \tag{3}$$

$$\mathcal{L} = \sum_{k=1}\mathcal{L}_k. \tag{4}$$

With the ETJASMIN pipeline, observation data from multiple instruments can be combined to increase the number of detectors and thus the statistics of the signal. For example, GECAM-B has 25 GRD detectors, while GBM (NaI only) and GECAM-C each have 12 detectors. If observations from all three spacecraft are available for a given source, the total number of detectors is up to 49.

The detection energy range of GECAM-B (Y. Q. Zhang et al. 2025, in preparation) and GECAM-C depends on the gain and bias voltage of each GRD (D. Zhang et al. 2022). Based on the calibration of the energy response (Y.-Q. Zhang et al. 2023), we select the optimal energy ranges for both high-gain and low-gain modes. For GBM, we use the energy range of 8–1000 keV for the joint search.

The entire sky is divided into equal-area pixels using the Hierarchical Equal Area iso-Latitude Pixelation (HEALPix) method.[14] With HEALPix, we set the total number of pixels to 3072, using a grid resolution parameter of $N_{\rm side} = 16$. Each pixel represents a specific sky location of a source and is associated with a unique instrument response matrix. The instrument response r_i corresponds to the expected, unnormalized source counts obtained by multiplying the spectral model by the instrument response matrix. Instrument responses are calculated for each sky location, resulting in 3072 LRs for each template spectrum. For a burst source with an unknown location, the LR varies with the source position, and we select the highest LR as the final result of the search. For a burst source with a known location, as provided by other instruments, the LR is computed using that specific location.

2.2.2. Simulation of Joint Search with Multiple Instruments

We implemented a series of Monte Carlo simulations to investigate the differences in detection sensitivity between individual spacecraft and multiple spacecraft using the coherent search method. Artificial data sets are created containing the background fluctuations in the individual detectors and energy channels based on the data from GECAM-B, GECAM-C, and Fermi-GBM. The mean background count rate is obtained by analyzing observed data from randomly selected periods using the GBM DATA Tools [15] and GECAM Tools.[16]

To assess the performance of the trigger algorithm through simulations, transient signals were superimposed onto the background. We simulated the expected burst signals detected by multidetectors and multichannels (25 GRD detectors and seven channels for GECAM-B, 12 GRD detectors and seven channels for GECAM-C, and 12 NaI detectors and four channels for GBM) using the response matrices of these three instruments from previous work (E. Bissaldi et al. 2009; R. Qiao et al. 2022; Y.-Q. Zhang et al. 2023). The simulated data sets were generated by sampling from a Poisson distribution, where the parameter λ (expectation) equals either the mean value of the background or the mean value of the background plus the burst signal. We assume an average spectral shape (e.g., Band spectrum) over the search timescale to calculate expected source counts and construct the likelihood function. For simplification, simulations assume uniform background across detectors from the same instrument, but actual analysis fits background levels separately for each detector and energy band for higher accuracy.

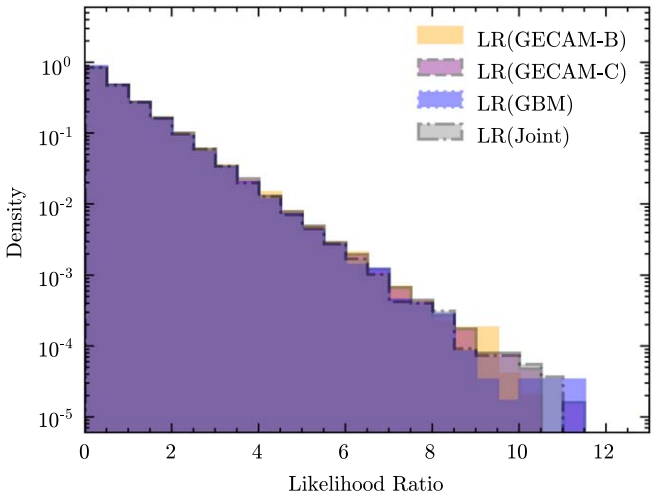

Figure 1. Simulated distributions for likelihood ratio of blind search using Poisson background alone. Orange, purple, blue, and gray represent GECAM-B search, GECAM-C search, GBM search, and a joint search of these three instruments, respectively.

To calibrate the corresponding confidence levels for a joint coherent search, four different search types were examined: GECAM-B search, GECAM-C search, GBM search, and joint search. This involved simulating the process of searching for approximately 10^5 transient signals in simulated light curves that included only Poisson noise. For each simulated data set, we performed a blind search across all possible directions (pixels) and template spectra, selecting the highest LR for each simulation. By repeating this simulation, we built a distribution of the maximum LR values (Figure 1). Additionally, we performed a targeted search using known directions and generated a corresponding distribution of LR values (Figure 2). For a specific observed LR value, the p-value is calculated as the proportion of simulations where the maximum LR exceeds the observed LR. For example, for a blind search with a specific LR value of 9, the corresponding confidence levels are 3.85σ, 3.85σ, 3.91σ, and 3.80σ for the GECAM-B search, GECAM-C search, GBM search, and joint search, respectively. This similarity allows for an intuitive comparison of absolute LR values to determine which search yields higher significance. This intuitive comparison is equally applicable to targeted search. Note that the LR distribution for blind search differs slightly from that of targeted search. Taking the joint search as an example (see Figure 3), for the same LR value, blind search yields lower significance. This is because the larger number of pixels in blind search increases the probability of finding false positives.

In this simulation, the duration, spectrum, and amplitude of the burst were set to 1 s, a standard Band spectrum (D. Band et al. 1993), and 0.006, respectively. The source amplitude,

[14] https://healpix.sourceforge.io/pdf/intro.pdf
[15] https://fermi.gsfc.nasa.gov/ssc/data/analysis/gbm/gbm_data_tools/gdt-docs/install.html
[16] https://github.com/zhangpeng-sci/GECAMTools-Public

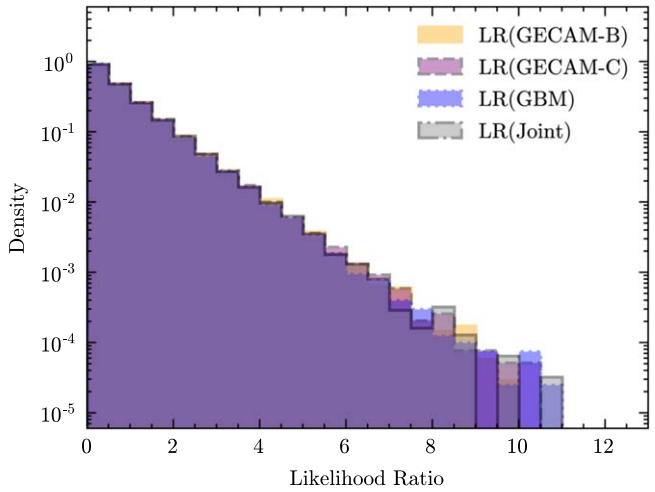

Figure 2. Simulated distributions for likelihood ratio of targeted search using Poisson background alone. Orange, purple, blue, and gray represent GECAM-B search, GECAM-C search, GBM search, and a joint search of these three instruments, respectively.

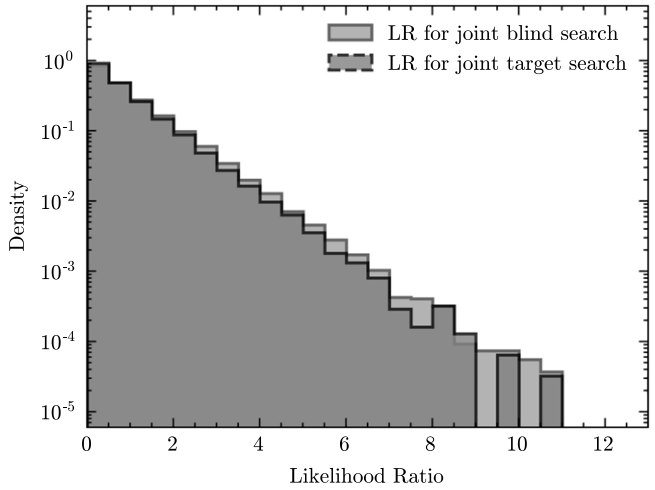

Figure 3. Simulated distributions for likelihood ratio using Poisson background alone. The solid line and dashed line represent the joint blind search and joint targeted search, respectively.

corresponding to a faint GRB with flux of 2.3×10^{-7} erg cm^{-2} s^{-1} (10–1000 keV), is used to simulate scenarios where the GRB signal is weak and challenging to detect, enabling the evaluation of multisatellite joint search performance in identifying faint GRBs. We also defined a source position with an R.A. of 137° and a decl. of 24° at the UTC time of 2022 November 26T13:07:29. This configuration was used to generate the simulated observed counts and unnormalized signals for the three satellites involved. The simulated observed source counts for each energy channel and detector over the specified duration are calculated by multiplying the spectral model (with a known amplitude) by the response matrix (depending on the source position). In contrast, the unnormalized signals are derived by multiplying the spectral model (with an unknown amplitude, i.e., 1) by the response matrix. Given the expected background ($\langle n_i \rangle$), unnormalized signal (r_i), and observed (simulated) counts (d_i), we can calculate the best amplitudes corresponding to maximum $\mathcal{L}$. To avoid the error of statistical fluctuations, the simulated observation data is set to the sum of the mean background and the mean signal values. The amplitudes of GECAM-B search, GECAM-C search, GBM search, and joint search are all 0.006, consistent with the preset values. The LR for the joint search is 76, which is higher than those for GECAM-B (20), GECAM-C (8), and GBM (47) searches. Since all four search types share the same background-only LR distribution, the absolute LR value directly indicates the significance of signal. Notably, the GBM search yields a higher LR than the GECAM search, influenced by factors such as the position and spectrum of the burst, the energy ranges, effective areas, and background levels of detectors.

We conducted a series of search simulations to evaluate the source amplitude estimation for joint search compared to individual satellite searches. It should be noted that the simulated data observed by GECAM-B, GECAM-C, and GBM were independently sampled, introducing statistical fluctuations in source amplitude estimates. The distributions of the source amplitude are shown in the left panel of Figure 4. The estimated amplitudes for all four types of searches consistently matched the expected value of 0.006, with some scatterings. The mean, standard deviation, and rms error of burst amplitude for the GECAM-B search, GECAM-C search, GBM search, and joint search are presented in Table 1. These results demonstrate that the joint search method exhibits less scattering compared to individual instrument searches, indicating a more precise estimation of the burst brightness. As shown in the right panel of Figure 4, the LR for the joint search surpasses that of the individual satellite searches. These results demonstrate the advantages of this novel transient detection algorithm with multiple instruments.

2.2.3. GRB Search

To demonstrate the performance of the search for GRBs of the ETJASMIN pipeline, the joint search for a GRB (taking GRB 221126A, for example) is performed on EVT/TTE data of GECAM-B, GECAM-C, and GBM. GRB 221126A was observed by GECAM-B, GECAM-C, and GBM at about 2022 November 26T13:07:29 UTC (A. von Kienlin et al. 2022). The light curves of these three instruments for this burst are shown in Figure 5. A joint search for GRB 221126A was conducted using the three instruments, with the results presented in Table 2. The search covers a series of timescales ranging from 0.05 to 4 s for GRBs. Three types of Band function (D. Band et al. 1993) are adopted as the typical GRB spectra incident to the instruments.

We note that, for the same search timescale, the source amplitude and spectrum template from the joint search are roughly consistent with those from individual satellite searches, while the joint LR from the three instruments is significantly larger than that of any single instrument. If the burst had been dimmed to approximately 10% of its original brightness, the joint search would still have detected this GRB with a maximum LR of 36.38, whereas GECAM-B or GECAM-C would likely have missed it, and GBM would have detected it with lower significance. These results demonstrate that the search method implemented in the ETJASMIN pipeline offers higher sensitivity for burst discovery.

2.2.4. SGR Search

The typical duration of short X-ray bursts from soft gamma repeaters (SGRs) ranges from about 0.1 to 1 s (A. C. Collazzi

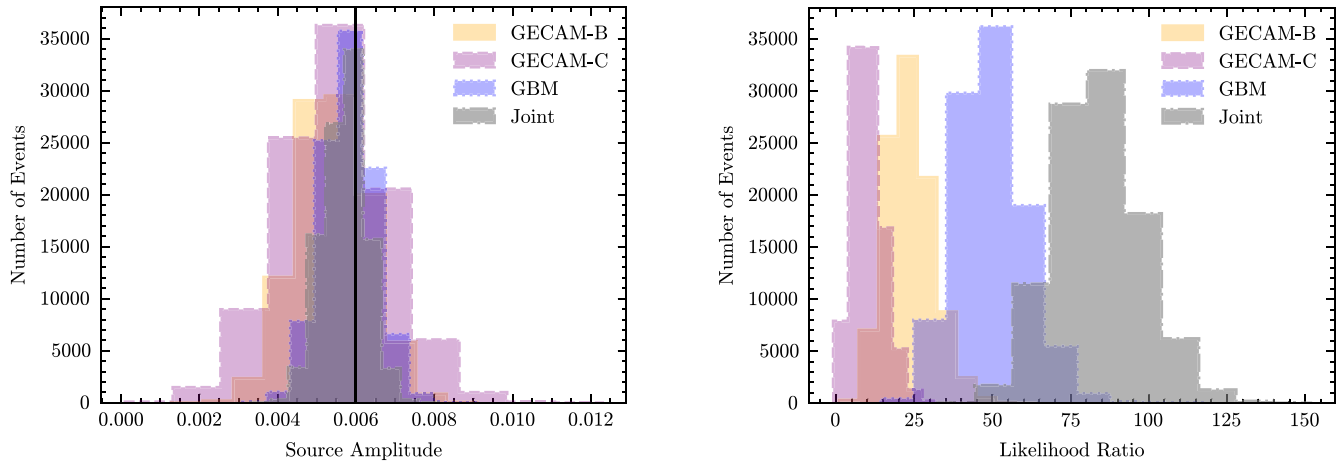

Figure 4. Orange, purple, blue, and gray represent GECAM-B search, GECAM-C search, GBM search, and a joint search of these three instruments, respectively. Left: the distribution of source amplitude based on the coherent search. The black line represents the preset source amplitude (the λ of Poisson distribution to generate the simulation data sets). Right: the distribution of LR based on the coherent search.

Table 1
Comparison of Burst Amplitude for Different Search Methods

Search Method	Mean	Standard Deviation	rms Error
GECAM-B search	5.4E–03	9.0E–04	1.1E–03
GECAM-C search	5.4E–03	1.4E–03	1.5E–03
GBM search	5.8E–03	6.5E–04	6.8E–04
Joint search	5.7E–03	5.3E–04	6.1E–04

et al. 2015; L. Lin et al. 2020; C. Cai et al. 2022a). Therefore, the joint search was performed on TTE/EVT data for SGR bursts on four timescales of 0.01, 0.02, 0.05, and 0.1 s. Five types of functions are adopted: Band function, power law (PL), cutoff power law (CPL), blackbody (BB), and OTTB as the SGR templates owing to their soft spectra (C. Cai et al. 2022a; S.-L. Xie et al. 2022).

The distance between GECAM-B, GECAM-C, and GBM typically ranges from a few hundred to about 10,000 km, causing a time delay of several to tens of milliseconds between the light curves detected by these two instruments. Given the short duration of SGR bursts (around a few milliseconds), it is essential to account for the light-travel time between the instruments.

Figure 6 shows the light curves of a burst from SGR J1935 +2154, which triggered both GBM and GECAM-B at 2021 September 12T05:14:07 UTC. Based on the position of SGR J1935+2145, we calculated the time delay of 0.01 s between GBM and GECAM-B at the trigger time. As shown in the bottom panel of Figure 6, the peak of the GBM light curve aligns with that of GECAM-B after correcting for this time delay.

We conducted a joint search for this SGR burst to estimate the impact of time delay between two instruments on the LR for short-duration bursts. Before correcting for the time delay, as shown in the top panel of Figure 6, the joint LR at the peak (2021 September 12T05:14:07.820 UTC) of GECAM-B and GBM was 424 with a 5 ms timescale, an amplitude of 0.03, and a soft Band spectrum template. The location of the maximum LR was R.A. 289.69, decl. 4.78. After applying the correction, the joint LR increased to 589 with the same timescale and template, and the location of the maximum LR shifted to R.A.

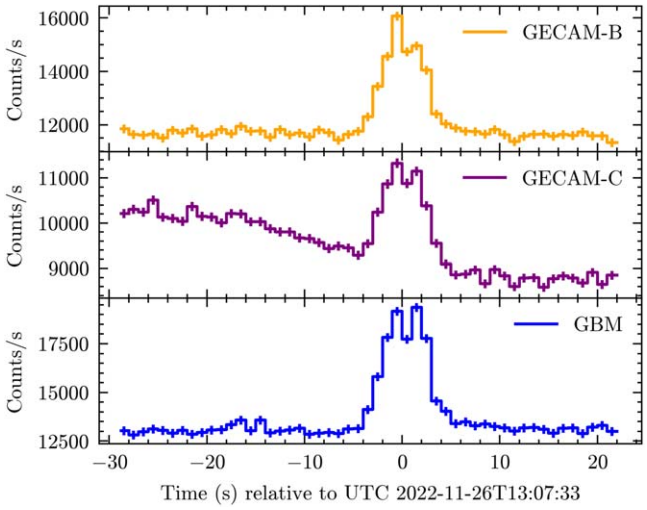

Figure 5. GECAM-B, GECAM-C, and GBM light curves of GRB 221126A. GECAM-C has high background level before the trigger time because it passed through the region of high particle activity.

302.75, decl. 19.83, closer to the true location of SGR J1935 +2154 (R.A. 293.732, decl. 21.89). The search results are summarized in Table 2. These results indicate that time delays between different instruments must be accounted for when jointly searching for short-duration bursts, such as SGR bursts with durations of approximately milliseconds.

2.2.5. Search for GWs' EM Counterparts

Searching for GWs' high-energy electromagnetic (EM) counterparts is desirable in the GW multimessenger era. Despite intensive searching efforts, GRB 170817A, a short-duration GRB lasting approximately 2 s, is still the unique high-energy EM counterpart of a GW event (GW170817) as of this writing (B. P. Abbott et al. 2017; A. Goldstein et al. 2017; V. Savchenko et al. 2017; T. Li et al. 2018). Therefore, we used the GRB parameters for the joint search for GW EM counterparts, as defined in Section 2.2.3.

During the first three observing runs (O1, O2, O3; B. P. Abbott et al. 2019; R. Abbott et al. 2021, 2023), no EM counterparts were detected, except for the confirmed

Table 2
The Result of Joint Search for GRBs, SGRs, and Particle Events

Source Name	UTC Time	Instruments	Timescale (s)	$\mathcal{L}$	S[a]	Spectrum[b]
GRB 20221126A	2022-11-26T13:07:33.000	GECAM-B	1	2324	0.049	Medium
	2022-11-26T13:07:33.000	GECAM-C	1	886	0.053	Medium
	2022-11-26T13:07:33.000	GBM	1	3463	0.047	Medium
	2022-11-26T13:07:33.000	GECAM-B + GECAM-C + GBM	1	6662	0.048	Medium
0.1 GRB 20221126A	2022-11-26T13:07:33.000	GECAM-B	1	11	0.0039	Medium
	2022-11-26T13:07:33.000	GECAM-C	1	3	0.0040	Medium
	2022-11-26T13:07:33.000	GBM	1	19	0.0037	Medium
	2022-11-26T13:07:33.000	GECAM-B + GECAM-C + GBM	1	36	0.0038	Medium
SGR J1935+2154[c]	2021-09-12T05:14:07.820	GECAM-B	0.005	0	0	...
	2021-09-12T05:14:07.820	GBM	0.005	463	0.05	Soft
	2021-09-12T05:14:07.820	GECAM-B + GBM	0.005	424	0.03	Soft
SGR J1935+2154[d]	2021-09-12T05:14:07.820	GECAM-B	0.005	109	0.036	Soft
	2021-09-12T05:14:07.820	GBM	0.005	472	0.065	Soft
	2021-09-12T05:14:07.820	GECAM-B + GBM	0.005	589	0.059	Soft
Swift J1555.2–5402	2021-06-03T09:45:46.674	GECAM-B	0.01	28	0.017	Soft
	2021-06-03T09:45:46.674	GBM	0.01	52	0.031	Soft
	2021-06-03T09:45:46.674	GECAM-B + GBM	0.01	86	0.027	Soft
A particle event	2023-02-06T08:47:04.100	GECAM-B	0.1	216	0.01	Hard
	2023-02-06T08:47:04.100	GBM	0.1	0.03	0.0004	Hard
	2023-02-06T08:47:04.100	GECAM-B + GBM	0.1	26	0.001	Hard

Notes.
[a] The source amplitude for a given spectral template.
[b] The spectral template (Band function) of the burst used in the search.
[c] The results of joint search for SGR J1935+2154 without correcting the time delay.
[d] The results of joint search for SGR J1935+2154 with correcting the time delay. The corrected GBM LR is different from that without correction owing to the different location of maximum LR between these two conditions.

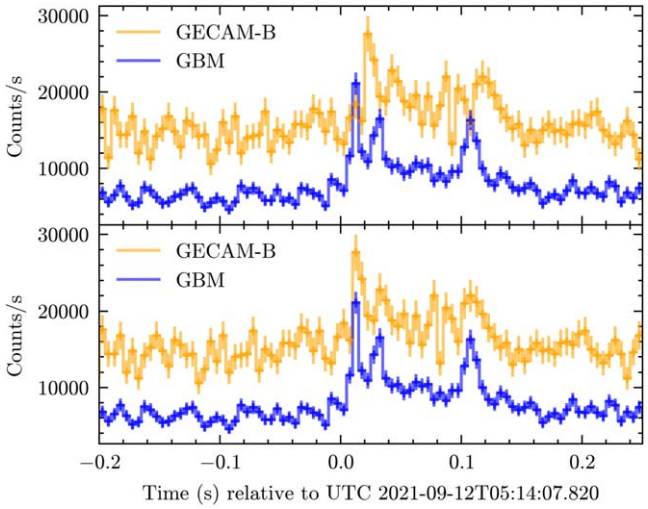

Figure 6. The light curves of SGR J1935+2154, observed by GECAM-B (orange lines) and GBM (blue lines). Top panel: the original light curves without correcting light-travel time. Bottom: the corrected light curves. The counts of GBM light curves are decreased by multiplying by a factor of 0.5.

association with the binary neutron star merger GW170817 using operational missions such as Fermi-GBM, Swift-BAT, and Insight-HXMT/HE.

Observing Run 4 (O4) started on 2023 May 24,[17] and it will continue for 20 calendar months from that date. Improvements in the sensitivity of the LIGO Hanford and Livingston, Virgo, and KAGRA (HLVK) interferometers have increased the detection rate (A. Colombo et al. 2022; P. Petrov et al. 2022), providing more opportunities to find gamma-ray transients associated with GW events.

S230518h is a significant detection candidate with a false-alarm rate of 3.2×10^{-10} Hz, classified with the highest probability as a neutron star–black hole (86%; Ligo Scientific Collaboration et al. 2023). Based on the location and trigger time of this candidate, we examined the data from GECAM-B, GECAM-C, and GBM, finding that GECAM-B had no observation available owing to Earth occultation or satellite passages through the South Atlantic Anomaly (SAA).

We utilized the joint search to examine a ± 30 s time window of GBM and GECAM-C data centered on the trigger time (2023 May 18T12:59:08 UTC) of S230518h to look for coincident signals in GBM and GECAM-C. No significant counterpart with an LR larger than 9 (roughly equivalent to a 3σ) was found by ETJASMIN (D. Kocevski et al. 2018; C. Cai et al. 2023).

In the case of nondetection of a burst, the 3σ upper-limit flux (10–1000 keV) was estimated with the ETJASMIN pipeline based on the available observations of targeted sources. To derive the optimized weighted light curve, as described in C. Cai et al. (2021b), the weighted factor can be estimated using the expected counts assuming different spectral models and the background at the GW trigger time. The normalization (corresponding to a 3σ SNR), together with other spectral parameters, is used to calculate the upper-limit flux with different timescales.

[17] https://emfollow.docs.ligo.org/userguide/capabilities.html

Table 3
GBM and GECAM-C Observation of S230518h in O4

Timescale (s)	Spectral Template	GECAM-C and GBM[a],[b] (erg cm^{-2} s^{-1})	GBM[b] (erg cm^{-2} s^{-1})
0.128	Soft	1.0E–07	1.4E–07
0.128	Norm	1.7E–07	2.7E–07
0.128	Hard	4.2E–07	6.1E–07

Notes.
[a] The 3σ upper-limit flux in 10–1000 keV with GBM and GECAM-C/GBM observation.
[b] The 3σ upper-limit flux from the GCN (S. Dalessi et al. 2023).

For S230518h, we estimate the upper limit using soft, normal, and hard Band spectrum templates with a timescale of 0.128 s, as shown in Table 3. The upper-limit flux on the timescale of 0.128 s using a soft Band spectrum template is 1.4×10^{-7} erg cm^{-2} s^{-1} with GBM data alone (S. Dalessi et al. 2023), whereas it improved to 1.0×10^{-7} erg cm^{-2} s^{-1} when combining GBM and GECAM-C data. These results demonstrate that the ETJASMIN pipeline provides a more stringent constraint on the upper limit of burst flux, as expected.

2.3. Burst Verification Analysis

Many subthreshold triggers from Fermi-GBM were released,[18] of which the observed flux is too weak for the trigger source to be verified. Similarly, subthreshold triggers from GECAM-B and GECAM-C are also difficult to identify. Verifying these weak burst candidates is critically important and very challenging.

With ETJASIN, we can collect weak and subthreshold triggers from multiple missions and search for them jointly using the coherent search method. For example, an unidentified burst source is triggered by Swift-BAT (D. M. Palmer et al. 2021) at UT 2021 June 03T09:45:46 and later confirmed as a new magnetar, Swift J1555.2–5402, using XRT data (P. A. Evans & Swift-XRT Team 2021). Soon after, GBM and GECAM-B also reported their subthreshold triggers (C. Cai et al. 2021a; C. Fletcher & Fermi-GBM Team 2021). The light curves from GBM and GECAM-B for this magnetar burst are shown in Figure 7.

If there were no observations from Swift for this burst, verifying this subtrigger as a magnetar burst using only GBM or GECAM-B observations proves challenging. According to the location of Swift J1555.2–5402 (R.A. 238.819, decl. –54.046; D. M. Palmer et al. 2021), we calculate the time delay of 0.004 s between GBM and GECAM at the trigger time UT 2021 June 3T09:45:46. After correcting for the time delay, we employed the ETJASIN pipeline to search for this subthreshold trigger, achieving an LR of 86 (which is quite significant and not a subthreshold event at all), with a timescale of 10 ms and a soft Band spectrum. The search results are listed in Table 2. Indeed, there is a statistical excess in the light curves of both GBM and GECAM-B simultaneously, indicating that the trigger originates from a real burst source. The location of the maximum LR for the joint search is consistent with the location of the magnetar Swift J1555.2–5402 provided by Swift. In addition, ETJASMIN provides time delay localization

[18] https://gcn.gsfc.nasa.gov/fermi_gbm_subthresh_archive.html

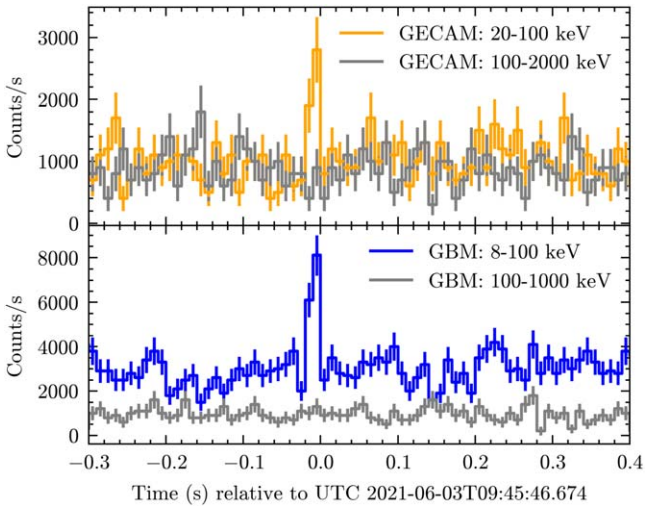

Figure 7. The light curves of SGR J1555.2–5402. Top panel: the 10 ms light curve of GECAM-B (GRD#5, 13, 21) in the energy ranges of 20–100 keV (orange line) and 100–2000 keV (gray line). Bottom panel: the 10 ms light curves of GBM (n9, na, and nb) in the energy ranges of 8–100 keV (blue line) and 100–1000 keV (gray line).

with GECAM-GBM-BAT, and the localized area is consistent with the precise position given by Swift, as discussed in Paper I of this series (S. Xiao et al. 2022). Therefore, the ETJASIN pipeline can effectively identify and verify this subthreshold trigger as a magnetar burst by jointly analyzing data from multiple missions, which is very difficult to achieve with an individual instrument (either GBM or GECAM-B).

2.4. Burst Classification Analysis

Many burst sources, including GRBs, solar flares, and charged particles (CPs), as well as instrumental effects, can make triggers in the gamma-ray instruments. Classifying these triggers is very important but usually difficult.

The Fermi-GBM and Insight-HXMT teams have released catalogs of GRBs (A. von Kienlin et al. 2020; X.-Y. Song et al. 2022). These catalogs show that, apart from GRBs, they also include other types of triggers, among which CPs are one of the main forms of contamination to the astrophysical bursts.

CPs are generally thought to be caused by the magnetospheric events interacting with the GRD. Magnetospheric events predominantly occur in regions of trapped particles that satellites traverse during their orbits, especially upon entering or exiting the SAA or at high geomagnetic latitude (e.g., North American). Therefore, CPs can be identified based on the position of the satellites when the trigger occurred.

At 2023 February 6T08:47:04.100 UTC, a particle event was detected by GECAM-B ground search with an LR of 216. The light curves for both GRDs and CPDs of GECAM-B are shown in Figure 8. The simultaneous detection of GRD and CPD of GECAM-B already shows that this burst is certainly not a gamma-ray transient; however, there are some instruments without CPD detectors (e.g., Fermi-GBM, GECAM-D), or the burst may be too weak to leave significant signal in CPDs.

Using the ETJASIN pipeline, we check the position of GECAM-B, GECAM-C, and GBM, as shown in Figure 9. GECAM-C EVT data were unavailable owing to the SAA passages of this satellite. The location of the particle event, corresponding to the maximum LR of GECAM-B, is shown in the sky map (Figure 10). The sky map indicates that neither

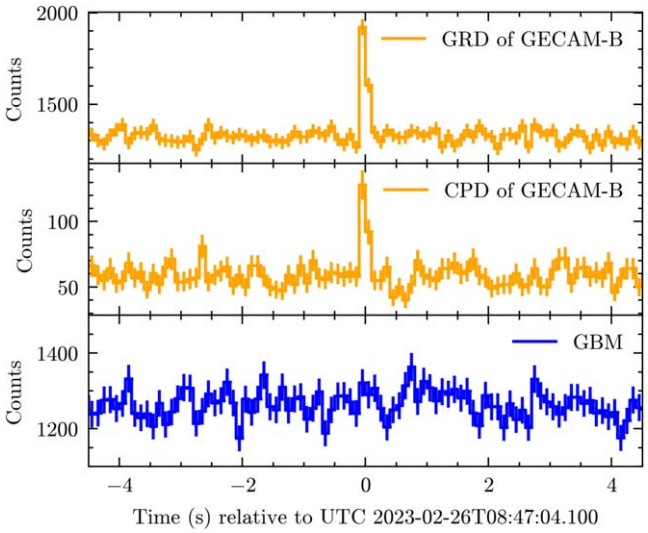

Figure 8. The light curves of a particle event, observed by GECAM-B (orange lines) and GBM (blue lines). Top panel: the GRD light curve of GECAM-B. Middle panel: the CPD light curve of GECAM-B. Bottom panel: the GRD light curve of GBM.

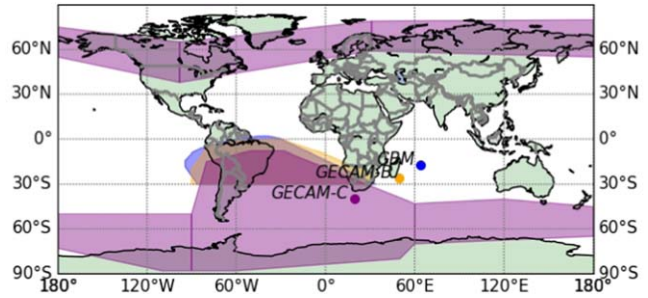

Figure 9. The position for a particle event of GECAM-B (yellow point), GECAM-C (purple point), and GBM (blue point), at the time of 2023 February 6T08:47:04.100 UTC. The blue, yellow, and purple shaded regions represent the SAA regions (i.e., trapped particle regions) of GECAM-B, GECAM-C, and GBM, respectively.

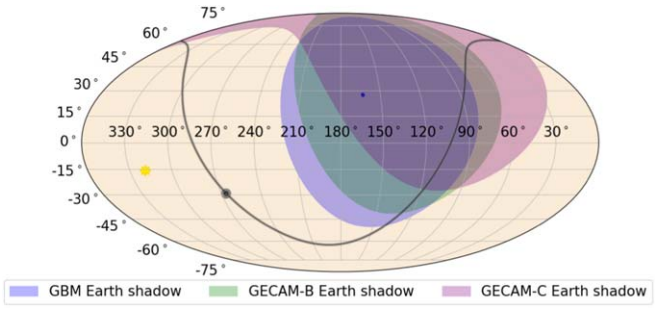

Figure 10. The sky map for a particle event of GECAM-B, GECAM-C, and GBM. The different colors of shaded regions represent the Earth occultation from different instruments at the time of 2023 February 6T08:47:04.100 UTC. The blue point is the location of this particle event from the GECAM ground search pipeline (C. Cai et al. 2025).

GBM nor GECAM-B is visible for this event, confirming that it is not a celestial source event. We search for this event using the data of GECAM-B and GBM, of which the LR at the peak time is 26. As noted in the bottom panel of Figure 8, there is no statistically significant excess in the GBM light curve, unlike the GECAM-B light curve. CPs rarely occur simultaneously in multiple instruments, due to the different trajectories of different satellites. Therefore, the LR for this type of event is significantly decreased in the joint search.

For this particle event, we compared the LR for GECAM-B, GBM, and their joint analysis, with LRs of 216 ($\mathcal{L}_{\rm gecam-b}$), 0.03 ($\mathcal{L}_{\rm gbm}$), and 26.94 ($\mathcal{L}$), respectively. The observed amplitudes of these three conditions (i.e., GECAM-B, GBM, and their joint analysis) are 0.01, 0.0004, and 0.001, respectively. While the source amplitude observed by different instruments generally shows slight variations due to differing sensitivities to GRBs, these should not be vastly different. For instance, if GECAM-B detects a GRB visible to GBM, the amplitude observed by GBM should be roughly in the same order of magnitude as that of GECAM-B. The search results are listed in Table 2. By comparing the source amplitudes from each instrument for which data are available, we can also eliminate CPs.

On the other hand, there is a type of instrumental effect that usually causes triggers in GRDs, called spikes. They appear as a brief increase in detected counts within the detector. C. Cai et al. (2021b) developed a method to eliminate spikes in the HXMT data, which are commonly observed in the light curves of gamma-ray instruments and usually occur in a single detector with high count rates. This method identifies these spike events by evaluating the ratio of the maximum LR of a single detector to the total LR summed in all detectors. Using this spike event filter, about 99% of the spike events are identified and removed, while almost all real GRBs are retained. This method is also integrated into the ETJASMIN pipeline to filter these spikes.

These results demonstrate that the ETJASMIN search pipeline inherently possesses the capability to classify GRB events apart from other events such as spikes and CPs.

3. Discussion and Conclusion

The main purpose of this series of papers is to propose, develop, and demonstrate the ETJASMIN pipeline, a specialized multi-instrument data analysis system designed to discover untriggered or subtriggered transient events (including GRBs, SGRs, and GW EM signals) using the data sets of GECAM series (GECAM-B, GECAM-C), as well as other gamma-ray instruments (e.g., Fermi-GBM). By integrating observation data from multiple instruments, ETJASMIN is more powerful, efficient, and accurate in the gamma-ray transient detection. As the second paper in this series on ETJASMIN, we focus on the burst search, verification, and classification, presenting the detailed methodology, procedures, and performance of the related data analyses.

For the burst search in ETJASMIN, we developed a coherent method based on the LR to jointly search for transients with GECAM-B, GECAM-C, and Fermi-GBM, which have similar energy response. Our extensive simulations provide evidence that this joint search estimates source brightness more accurately and achieves higher significance of burst detection (Figures 1–4).

Using ETJASMIN, we showed the GRB search with a typical burst, GRB 221126A (Figure 5), and a faint burst with 10% of the brightness of GRB 221126A, jointly observed by GECAM-B, GECAM-C, and Fermi-GBM. The results show that the joint LR of these three instruments is significantly higher than that of the individual spacecraft, and their respective estimated source amplitudes are consistent with each other (Table 2). These results confirm that the joint search

has higher sensitivity to detect GRBs than the individual spacecraft searches.

Regarding the SGR burst search, we searched for a short-duration burst from SGR J1935+2154 (Figure 6), jointly observed by GECAM-B and Fermi-GBM, and found that the time delay between different instruments reduces detection significance for signals lasting only a few milliseconds. Once the time delay is corrected, the sensitivity for SGR bursts can be improved through joint search. Additionally, we searched for GW EM counterparts and estimated the upper-limit flux using ETJASMIN, showing that this multi-instrument pipeline can provide a more stringent constraint on the upper-limit flux.

Within the ETJASMIN framework, multiple GRB missions (such as GECAM-B, GECAM-C, and GBM) can be used to jointly verify weak transients and subthreshold candidates. Joint detection of subthreshold events (such as the Swift J1555.2–5402 burst; Figure 7) in multiple instruments can significantly enhance their confidence.

The results presented in Section 2.4 highlight the effectiveness of classifying CP events by comparing estimated source brightness across multiple instruments (see Figure 8). Typically, when multiple instruments with similar response detect a genuine astrophysical transient (e.g., GRB, SGR), the observed source brightness should remain within a comparable range despite differences in sensitivity of individual instruments. The ability of the ETJASMIN pipeline to identify such inconsistencies across instruments is crucial for distinguishing nonastrophysical bursts (e.g., CP events) from astrophysical signals.

These results also indicate that ETJASMIN is particularly suitable for the search and verification of weak gamma-ray transients, including the short and/or faint GRBs and SGR bursts, especially those associated with GW and FRB events. Detailed and systematic search, verification, and classification of gamma-ray transients with ETJASMIN will be implemented and reported in the forthcoming work.

Acknowledgments

We thank the anonymous reviewer for very helpful comments and suggestions. This work is supported by the National Natural Science Foundation of China (grant No. 12303045, 12273042, 12373047), the National Key R&D Program of China (2022YFF0711404, 2021YFA0718500), and the Strategic Priority Research Program of Chinese Academy of Sciences (grant Nos. XDA15360102, XDA15360300, XDA30050000, XDB0550300). The GECAM (Huairou-1) mission is supported by the Strategic Priority Research Program on Space Science (grant No. XDA15360000) of the Chinese Academy of Sciences. C.C. acknowledges the support from the Hebei Natural Science Foundation (No. A2023205020) and the Science Foundation of Hebei Normal University (No. L2023B11).

ORCID iDs

Ce Cai https://orcid.org/0000-0002-6540-2372
Shao-Lin Xiong https://orcid.org/0000-0002-4771-7653

References

Abbott, B. P., Abbott, R., Abbott, T. D., et al. 2016, PhRvL, 116, 131103
Abbott, B. P., Abbott, R., Abbott, T. D., et al. 2019, PhRvX, 9, 031040
Abbott, B. P., Abbott, R., Abbott, T. D., et al. 2017, PhRvL, 119, 161101
Abbott, R., Abbott, T. D., Abraham, S., et al. 2021, PhRvX, 11, 021053
Abbott, R., Abbott, T. D., Acernese, F., et al. 2023, PhRvX, 13, 041039
Abramovici, A., Althouse, W. E., Drever, R. W. P., et al. 1992, Sci, 256, 325
Accadia, T., Acernese, F., Alshourbagy, M., et al. 2012, JInst, 7, 3012
An, Z.-H., Antier, S., Bi, X.-Z., et al. 2023, arXiv:2303.01203
An, Z. H., Sun, X. L., Zhang, D. L., et al. 2022, RDTM, 6, 43
Aptekar, R. L., Frederiks, D. D., Golenetskii, S. V., et al. 1995, SSRv, 71, 265
Band, D., Matteson, J., Ford, L., et al. 1993, ApJ, 413, 281
Barthelmy, S. D., Barbier, L. M., Cummings, J. R., et al. 2005, SSRv, 120, 143
Bissaldi, E., von Kienlin, A., Lichti, G., et al. 2009, ExA, 24, 47
Blackburn, L., Briggs, M. S., Camp, J., et al. 2015, ApJS, 217, 8
Bochenek, C. D., Ravi, V., Belov, K. V., et al. 2020, Natur, 587, 59
Cai, C., Xiong, S. L., Huang, Y., et al. 2021a, GCN, 30140, 1
Cai, C., Xiong, S.-L., Lin, L., et al. 2022a, ApJS, 260, 25
Cai, C., Xiong, S.-L., Xue, W.-C., et al. 2023, MNRAS, 518, 2005
Cai, C., Xue, W.-C., Li, C.-K., et al. 2022b, ApJS, 260, 24
Cai, C., Xiong, S. L., Li, C. K., et al. 2021b, MNRAS, 508, 3910
Cai, C., Zhang, Y. Q., Xiong, S. L., et al. 2025, SCPMA, 68, 239511
Cao, X., Jiang, W., Meng, B., et al. 2019, SCPMA, 63, 249504
Chen, Y., Cui, W., Li, W., et al. 2019, SCPMA, 63, 249505
Chen, Y.-P., Li, J., Xiong, S.-L., et al. 2022, ApJ, 935, 10
CHIME/FRB Collaboration, Andersen, B. C., Bandura, K. M., et al. 2020, Natur, 587, 54
Collazzi, A. C., Kouveliotou, C., van der Horst, A. J., et al. 2015, ApJS, 218, 11
Colombo, A., Salafia, O. S., Gabrielli, F., et al. 2022, ApJ, 937, 79
Connaughton, V., Burns, E., Goldstein, A., et al. 2016, ApJL, 826, L6
Dalessi, S., Fletcher, C. & Fermi-Gbm TeamGbm-Ligo/VIRGO/Kagra Group 2023, GCN, 33818, 1
Dong, Y., Wu, B., Li, Y., Zhang, Y., & Zhang, S. 2010, SCPMA, 53, 40
Evans, P. A. & Swift-XRT Team 2021, GCN, 30122, 1
Feng, P.-Y., An, Z.-H., Zhang, D.-L., et al. 2024, SCPMA, 67, 111013
Fletcher, C. & Fermi-GBM Team 2021, GCN, 30125, 1
Goldstein, A., Burns, E., Hamburg, R., et al. 2016, arXiv:1612.02395
Goldstein, A., Veres, P., Burns, E., et al. 2017, ApJL, 848, L14
Goldstein, A., Hamburg, R., Wood, J., et al. 2019, arXiv:1903.12597
Greiner, J., Burgess, J. M., Savchenko, V., & Yu, H. F. 2016, ApJL, 827, L38
Kerr, M., Duvall, W., Johnson, W. N., et al. 2023, ApJ, 953, 24
Kocevski, D., Burns, E., Goldstein, A., et al. 2018, ApJ, 862, 152
Li, C. K., Lin, L., Xiong, S. L., et al. 2021, NatAs, 5, 378
Li, T., Xiong, S. L., Zhang, S. N., et al. 2018, SCPMA, 61, 031011
Li, X. Q., Wen, X. Y., An, Z. H., et al. 2022, RDTM, 6, 12
Ligo Scientific Collaboration, VIRGO Collaboration, Kagra Collaboration 2023, GCN, 33813, 1
Lin, L., Göğüş, E., Roberts, O. J., et al. 2020, ApJL, 902, L43
Liu, C. Z., Zhang, Y. F., Li, X. F., et al. 2019, SCPMA, 63, 249503
Lv, P., Xiong, S., Sun, X., Lv, J., & Li, Y. 2018, JInst, 13, P08014
Meegan, C., Lichti, G., Bhat, P. N., et al. 2009, ApJ, 702, 791
Mereghetti, S., Savchenko, V., Ferrigno, C., et al. 2020, ApJL, 898, L29
Palmer, D. M., Evans, P. A., Kuin, N. P. M., Page, K. L. & Swift Team 2021, GCN, 30120, 1
Petrov, P., Singer, L. P., Coughlin, M. W., et al. 2022, ApJ, 924, 54
Qiao, R., Guo, D. Y., Peng, W. X., et al. 2022, RAA, 24, 104005
Qie, X., Guo, S., He, J., et al. 2021, in 2021 IEEE 15th Int. Conf. on Electronic Measurement & Instruments (ICEMI) (Piscataway, NJ: IEEE), 254
Rau, A., Kienlin, A. V., Hurley, K., & Lichti, G. G. 2005, A&A, 438, 1175
Ridnaia, A., Svinkin, D., Frederiks, D., et al. 2021, NatAs, 5, 372
Savchenko, V., Ferrigno, C., Kuulkers, E., et al. 2017, ApJL, 848, L15
Song, X.-Y., Xiong, S.-L., Zhang, S.-N., et al. 2022, ApJS, 259, 46
Tavani, M., Casentini, C., Ursi, A., et al. 2021, NatAs, 5, 401
von Kienlin, A., Meegan, C. & Fermi GBM Team 2022, GCN, 32994, 1
von Kienlin, A., Meegan, C. A., Paciesas, W. S., et al. 2020, ApJ, 893, 46
Wang, C., Zhang, Y., Xiong, S., et al. 2024a, ChJSS, 44, 668
Wang, C., Zhang, J., Zheng, S., et al. 2024b, ExA, 57, 26
Wen, J., Long, X., Zheng, X., et al. 2019, ExA, 48, 77
Xiao, S., Xiong, S.-L., Cai, C., et al. 2022, MNRAS, 514, 2397
Xie, S.-L., Cai, C., Xiong, S.-L., et al. 2022, MNRAS, 517, 3854
Xiong, S. 2016, arXiv:1605.05447
Xu, Y. B., Li, X. Q., Sun, X. L., et al. 2022, RDTM, 6, 53
Zhang, D., Li, X., Wen, X., et al. 2022, NIMPA, 1027, 166222
Zhang, D., Zheng, C., Liu, J., et al. 2023, NIMPA, 1056, 168586
Zhang, D. L., Gao, M., Sun, X. L., et al. 2022, RDTM, 6, 35
Zhang, S. N., Li, T. P., Lu, F. J., et al. 2019, SCPMA, 63, 249502
Zhang, Y.-Q., Xiong, S.-L., Mao, J.-R., et al. 2024, SCPMA, 67, 289511
Zhang, Y.-Q., Xiong, S.-L., Qiao, R., et al. 2023, arXiv:2303.00698
Zhao, H.-S., Li, D., Xiong, S.-L., et al. 2023, SCPMA, 66, 259611
Zhao, X.-Y., Xiong, S.-L., Wen, X.-Y., et al. 2021, arXiv:2112.05101
Zheng, C., An, Z.-H., Peng, W.-X., et al. 2024, NIMPA, 1059, 169009